Vesicular reuptake inhibition by a synaptotagmin I C2B domain antibody at the squid giant synapse

Rodolfo R. Llinás*[†‡], Mutsuyuki Sugimori*[‡], Kimberly A. Moran*[‡], Jorge E. Moreira[‡§], and Mitsunori Fukuda[‡¶]

*Department of Physiology and Neuroscience, New York University School of Medicine, 550 First Avenue, New York, NY 10016 ; §Department of Cell and Molecular Biology, Riberão Preto School of Medicine, University of São Paulo, CEP 3900, São Paulo, Brazil; ¶Fukuda Initiative Research Unit, RIKEN, 2-1 Hirosawa, Wako, Saitama 351-0198, Japan; and ‡Marine Biological Laboratory, Woods Hole, MA 02543

Synaptotagmin (Syt) I, a ubiquitous synaptic vesicle protein, comprises a transmembrane region and two C2 domains. The C2 domains, which have been shown to be essential for both synaptic vesicle exocytosis and endocytosis, are also seen as the Ca^{2+} sensors in synaptic vesicular release. In a previous study, we reported that a polyclonal antibody raised against the squid (*Loligo pealei*) Syt I C2B domain, while inhibiting vesicular endocytosis, was synaptic release neutral at the squid giant synapse. Recent reports concerning the C2B requirements for synaptic release prompted us to readdress the role of C2B in squid giant synapse function. Presynaptic injection of another anti-Syt I-C2B antibody (using recombinant whole C2B domain expressed in mammalian cell culture as an antigen) into the presynaptic terminal reproduced our previous results, i.e., reduction of vesicular endocytosis without affecting synaptic release. This set of results addresses the issue of the geometrical arrangement of the Ca^{2+} sensor, allowing the C2B domain antibody to restrict Ca^{2+}-dependent C2B self-oligomerization without modifying the Ca^{2+}-dependent release process.

mollusk | presynaptic | synaptic transmission

Genetic, biochemical, and physiological studies during the past decade have indicated that synaptotagmin (Syt) I, an abundant synaptic vesicle protein, is an essential constituent of efficient Ca^{2+}-dependent exocytosis and endocytosis of synaptic vesicles (1–5). Syt I has two cytoplasmic Ca^{2+}-binding domains (a membrane-proximal C2A domain and a membrane-distal C2B domain) that are thought to function differently by means of binding to their specific ligand(s) during the synaptic vesicle cycle (5–10). Basically, this notion reached by using, among other techniques, domain-specific antibody- or peptide-injection experiments (6–10), and by analysis of *syt I*-null mutant animals (11–14). The antibody against the C2A domain blocks fusion step of synaptic vesicles (7, 8), whereas the antibody against the C2B domain blocks synaptic vesicle recycling but has no effect on synaptic vesicle exocytosis (9); although involvement of the C2B domain in the synaptic vesicle fusion step has been suggested (15–23).

Three recent findings about the Syt I C2B domain have lead us to reevaluate the role of the anti-Syt I-C2B antibody in neurotransmitter release: (*i*) The three-dimensional structure of the C2B domain indicates a larger than previously expected domain size where the short C terminus of the Syt family must be a part of the C2B domain (i.e., β8 strand; see Fig. 1*C*) (24, 25). Because the short C terminus was first proposed to be an independent domain [based on sequence comparisons with the C2A domain structure (26)], we previously used recombinant C2B domain lacking the β8 strand for antibody production (9, 27). (*ii*) Because the β8 strand is essential for proper folding of the C2B domain (28), in its absence, the truncated C2B domain tends to misfold in living cells and is less stable than the wild-type protein (28). More importantly, the truncated C2B domain exhibits somewhat different biochemical properties compared with native protein in terms of ligand binding specificity and affinity. (*iii*) Recombinant C2B domain purified from bacteria could be contaminated by nonproteinaceous components, resulting in the contradictory reports on the *in vitro* binding activity of the C2B domain (29).

Here, we produce an antibody against the C2B domain of Syt I (henceforth referred to as anti-mSyt I-C2B), by using a whole C2B domain purified from a mammalian cell culture as an antigen, and examined its effect on synaptic vesicle trafficking in the squid giant synapse by electrophysiological techniques, two-photon confocal imaging, and electron microscopy.

Materials and Methods

Expression Constructs and Transfection. pEF-T7-Syt I-cyto [amino acid residues 88–424 of squid Syt I (7)], pEF-T7-Syt I-C2A (amino acid residues 145–274 of squid Syt I), pEF-T7-Syt I-C2B (amino acid residues 274–424 of squid Syt I), and pEF-T7-GST-Syt I-C2B were constructed by using conventional PCR techniques, and all constructs were verified by DNA sequencing with the Hitachi SQ-5500 DNA sequencer as described (30, 31). Plasmid DNA was prepared by using Qiagen (Valencia, CA) Maxi prep kits. Transfection of pEF-Syt constructs into COS-7 cells (7.5×10^5 cells, the day before transfection per 10-cm plate) was achieved with Lipofectamine Plus reagent according to the manufacturer's notes (Invitrogen).

Production of Anti-mSyt I-C2B Antibody. Because native Syt I undergoes various posttranslational modifications (32), and recombinant proteins from bacteria were often contaminated by nonproteinaceous components, we used a mammalian cell expression system rather than a bacterial expression system to produce recombinant C2B domain (31, 33). Three days after transfection, COS-7 cells (20 10-cm dishes) expressing recombinant T7-GST-mSyt I-C2B were harvested and then homogenized in 10 ml of PBS (containing 0.1 mM phenylmethylsulphonyl fluoride, 10 μM leupeptin, and 10 μM pepstatin A) in a glass-Teflon Potter homogenizer with 10 strokes at 1,000 rpm. After solubilization with 1% Triton X-100 at 4°C for 1 h, the supernatants were obtained by centrifugation at $17,400 \times g$ for 10 min. Glutathione Sepharose 4B beads (Amersham Pharmacia Biosciences, Buckinghamshire, U.K.; wet volume, 50 μl) were added to the supernatants, followed by incubation at 4°C for 1 h with gentle agitation, after which the beads were washed with 10 ml of PBS containing protease inhibitors. T7-GST-mSyt I-C2B was eluted from the beads by incubation with 5 mM glutathione and 50 mM Tris·HCl, pH 7.5, and then the purified protein was extensively dialyzed against PBS.

New Zealand White rabbits were immunized with the purified GST-mSyt I-C2B ($\approx$ 50–100 μg) with Ribi adjuvant (Corixa, Hamilton, MT) as described (34). After removal of the cross-reactivity with GST and the short C terminus by incubating with 1 mg of GST-Syt-C terminus (amino acid residues 397–424 of

---

Abbreviations: Syt, synaptotagmin; ICa, Ca^{2+} current; CCV, clathrin-coated vesicle.

[†]To whom correspondence should be addressed. E-mail: llinar01@popmail.med.nyu.edu.

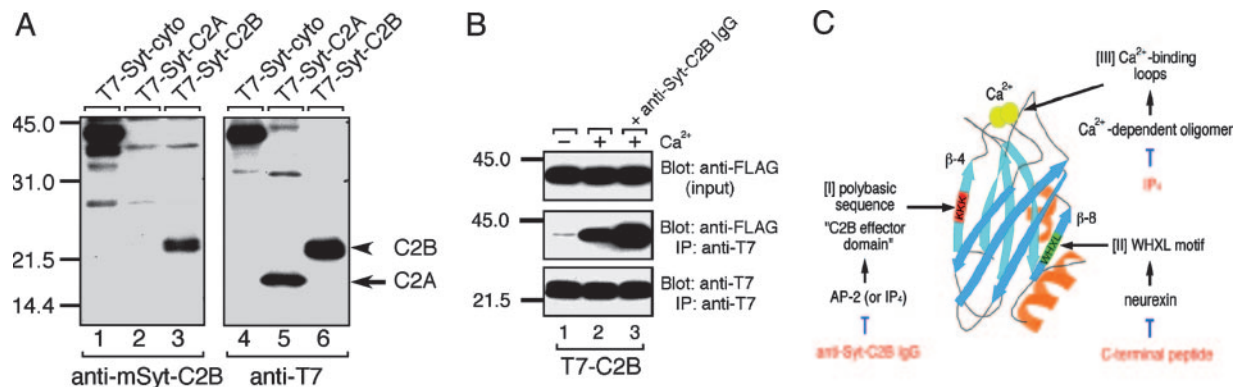© 2004 by The National Academy of Sciences of the USA

NEUROSCIENCE

Fig. 1. Characterization of the anti-mSyt I-C2B antibody. (*A*) Immunoblots showing the specificity of the anti-mSyt I-C2B with the total homogenates of COS-7 cells expressing T7-Syt I-cyto, T7-Syt I-C2A, or T7-Syt I-C2B. Recombinant T7-tagged Syts were subjected to SDS/12.5% PAGE and transferred to a poly(vinylidene difluoride) membrane. The blots were first probed with the anti-mSyt I-C2B antibody (0.5 μg/ml; *Left*). The same blots were stripped and reprobed with HRP-conjugated anti-T7 tag antibody (1/10,000 dilution) to ensure loading of the same amounts of T7-Syt proteins (*Right*). Note that the anti-mSyt I-C2B antibody specifically recognized the C2B domain (lane 3), but not the C2A domain (lane 2), even after prolonged exposure to x-ray film (data not shown). (*B*) Effect of the anti-mSyt I-C2B antibody on Ca^{2+}-dependent oligomerization of the C2B domain. Purified T7-mSyt I-C2B domain (*Bottom*) was coupled with the anti-T7 tag antibody-conjugated agarose and incubated with FLAG-Syt cytoplasmic domain in the presence of 2 mM EGTA (lane 1) or 1 mM Ca^{2+} (lanes 2 and 3) (30, 31). After the beads were washed extensively, proteins bound to the beads were analyzed by SDS/12.5% PAGE, followed by immunoblotting with HRP-conjugated anti-FLAG tag antibody (*Middle*). Input means 1/80 volume of the reaction mixture (*Top*). Note that the anti-mSyt I-C2B antibody (10 μg) did not inhibit Ca^{2+}-depenent oligomerization of the C2B domain (Lane 3, *Middle*); instead, it promoted oligomerization. The positions of the molecular mass markers ($\times 10^{-3}$) are shown on the left. (*C*) Schematic representation of the three distinct ligand-binding sites of the C2B domain (5, 25).

squid Syt I), anti-mSyt I-C2B antibody was affinity-purified by exposure to antigen-bound Affi-Gel 10 beads (Bio-Rad) as described (34). Specificity of the antibody was checked by immunoblotting, using recombinant T7-tagged C2A and C2B expressed in COS-7 cells (see Fig. 1*A*). SDS/PAGE and immunoblot analyses were performed as described (30). The blots shown in this paper are representative of two independent experiments. Conjugation of IgG with 5-carboxyfluorescein (Molecular Probes, catalog no. C-2210) was performed according to the manufacturer's instructions (7, 35).

Electrophysiology. The isolation of the squid stellate ganglion, electrophysiological techniques, and protocol, as well as the composition of the continuously superfused artificial seawater, was the same as in our previous experiments (6). The database comprises 45 preparations that were successfully studied. Of these preparations, 34 were injected with anti-mSyt I-C2B IgG and 3 were injected with denatured IgG. The controls ($n = 8$) reproduced the experimental protocol without IgG injection. Electrophysiological recordings were obtained with microelectrodes filled with a mixture of cesium chloride and tetraethylammonium chloride for voltage-clamp studies or with potassium citrate for other studies. The presynaptic and postsynaptic terminals were impaled with recording and current-injecting microelectrodes.

Noise analysis ($n = 4$) was implemented by using the procedures described in detail in previous work from our laboratory (36). Synaptic noise was recorded from the giant postsynaptic axon by using a high-gain ($\times 10,000$) low-noise AC-coupled amplifier using 10-kH sampling. A typical segment consisted of 16,000 data points. These segments were each divided into 1,024 points that were then cosine-tapered (36) for further analysis. Each segment was fast Fourier-transformed and the resultant spectra were averaged. The tapering effect on the magnitude of the power spectrum was then corrected. The same procedure was followed for analysis of the extracellular noise spectrum.

Voltage-Clamp Experiments. Voltage-clamp experiments ($n = 15$) involved double presynaptic implement of the preterminal (37). The ionic currents responsible for spike generation (e.g., voltage-gated sodium and potassium conductances) were blocked by

tetrodotoxin and tetraethylammonium, respectively. Ca^{2+} currents were activated by using voltage steps from a 70-mV holding potential. The Ca^{2+} currents were leakage-subtracted and monitored for the duration of the experiment.

Presynaptic Microinjection. Injection fluid containing 500 mM potassium acetate, 100 mM Hepes (pH 7.2), and 2–5 mg of 5-carboxyfluorescein-conjugated anti-mSyt I-C2B per ml, was pressure-injected into the presynaptic terminal. The progression of the labeled IgG into the terminal digit was monitored at 10-min intervals for the duration of the experiment by using fluorescent microscopy, and was recorded in a video frame grabber (Argus 100, Hamamatsu Photonics, Hamamatsu, Japan). This procedure monitored the diffusion of the IgG into the terminal and allowed it to be correlated with changes in postsynaptic response amplitude.

Two-Photon Microscopy. Immediately after the electrophysiological study, 10 of the 45 stellate ganglia were rapidly placed in a seawater chamber suitable for use with an inverted two-photon laser-scanning microscope. The instrument used was a Leica microscope system with a $20\times$ and a $63\times$ water-immersion objective lens. The krypton/argon laser system was adjusted to emit at 820 nm, and the two-photon absorption resulted in a wavelength of 410 nm at the focal point of the objective lens. Imaging of the distribution of the labeled anti-mSyt I-C2B demonstrated clear localization of the IgG at the presynaptic plasmalemma with a distribution consistent with the localization of the synaptic active zones in this junction.

Ultrastructure. After electrophysiological recording, those ganglia not used for two-photon microscopy ($n = 12$) were removed from the recording chamber and fixed by immersion in 6% glutaraldehyde in Ca^{2+}-free seawater, postfixed in osmium tetroxide, and in-block-stained with uranyl acetate (7). They were dehydrated in ethanol, substituted with propylene oxide, and embedded in Araldite resin (CY212) or Embed 812 (EM Science). Ultrathin sections were collected on Pyoloform (Ted Pella, Redding, CA) and carbon-coated single-sloth grids, contrasted with uranyl acetate and lead citrate, observed, and digitally photographed in a JEOL 200CX transmission electron
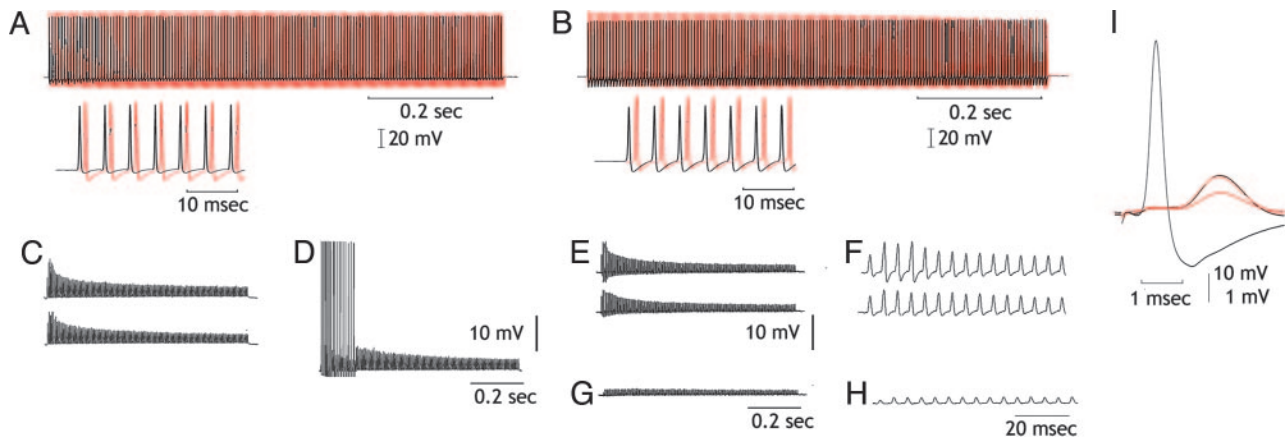
Fig. 2. Effect of intracellular C2B IgG injection in transmitter availability. (*A* and *B*) Upper traces, simultaneous presynaptic (black) and postsynaptic (red) recordings after repetitive presynaptic stimulation at 200 Hz. Lower traces are as above at higher sweep speed. (*C*) Control, the stimulus trains are repeated until all post spikes fail (upper trace). Trains are repeated every 5 sec until all spikes fail at the first stimulus train after 5-sec pause (lower trace). (*D*) After 15 min, stimulus train demonstrates recovery from transmitter depletion. (*E*) The same as in *C* but after IgG injection. (*F*) Postsynaptic potentials shown at higher gain and sweep speed to show detail time course. (*G*) Transmission after 15-min rest interval, demonstrating further reduction of transmitter release. (*H*) The same as in *G* but at a higher sweep speed. (*I*) Detailed comparison of the last synaptic potential in *F* (upper trace) and *H* to show amplitude reduction but no change in synaptic time course as the smaller potential is enlarged (red) to the amplitude of the potential in *F* (black).

microscope adapted with an AMT digital camera. Electron micrographs were taken at initial magnifications of ×10,000–30,000. Morphometry and quantitative analysis of the synaptic vesicles were performed with in-house program designed in LABVIEW for vesicle counting and density determination. Vesicle density was determined as number of vesicles per μm^2. Docked vesicles were identified as those vesicles in contact with the presynaptic membrane of each cluster. Statistical analyses of the data were performed by using GRAPHPAD INSTAT software. Significant values were calculated by using a Kruskal–Wallis test (nonparametric ANOVA).

Results

Preparation of Specific Antibody Against the Whole C2B Domain Produced by Mammalian Expression System. In a previous study (9), we showed that the anti-bSyt I-C2BΔβ8 antibody (against the bacterial recombinant C2B domain lacking the β8 strand) specifically inhibits synaptic vesicle recycling step but has no effect on synaptic vesicle docking and fusion. However, recent crystallographic analysis indicates that our previous recombinant C2B domain from bacteria, used as an antigen, lacks the C terminus of the C2B domain (corresponding to the β8 strand) (24, 25) (Fig. 1*C*), and accordingly, the recombinant C2B domain lacking the β8 strand may not fully inhibit the function of the C2B domain *in vivo*. To address this issue, we produced another anti-Syt I-C2B antibody by using recombinant whole C2B domain expressed in mammalian cell culture as an antigen (see *Materials and Methods* for details). As shown in Fig. 1*A*, the anti-mSyt I-C2B antibody specifically recognized the C2B domain and whole-cytoplasmic domain, but not the C2A domain (lanes 3 and 6, arrowhead).

Effect of Anti-mSyt I-C2B IgG Injection on Synaptic Vesicle Trafficking: Electrophysiological Analysis. We examined the effect of anti-mSyt I-C2B on neurotransmitter release at the giant synapse. As in our previous study (9), no effect was observed on transmitter release; even 1 h after the presynaptic terminal was total filled with anti-mSyt I-C2B, as confirmed by fluorescence imaging (*n* = 5). As illustrated in Fig. 2, the amplitude and latency of the postsynaptic response was not modified after presynaptic anti-mSyt I-C2B IgG injection and followed for a period up to 2 h (Fig. 2 *A* and *B*). These results demonstrate that the IgG

injection does not interfere with the synaptic release mechanism, confirming similar findings with a different antibody. This finding is important because it addresses the issue of C2B domain role in transmitter release.

Transmitter Availability. A set of experiments was designed to test the vesicular reuptake properties of the injected synapses to find whether anti-mSyt I-C2B IgG modified transmitter availability. After injection of the anti-mSyt I-C2B IgG, trains of presynaptic spikes were delivered and the postsynaptic response amplitude was used as a test for vesicular reuptake (Fig. 2). Trains of presynaptic spikes (200 Hz for 750 msec, 150 spikes) were delivered at 5-sec intervals until all synaptic activation was subthreshold for spike initiation (Fig. 2*E*). The synapse was then allowed to rest for 5 min. This routine was continued until a large, and sometimes complete, reduction of transmitter release was observed (Fig. 2*G*). No recuperation of transmitter release was observed in any of the six preparations tested after a 30-min rest period (Fig. 2*I*). To test whether the reduction of transmitter availability was due to the anti-mSyt I-C2B IgG, an aliquot of the IgG was boiled for 10 min and injected into three different synapses. Eight other synapses were used as uninjected controls. In all 11 experiments, synaptic transmitter release returned to normal after 30-min rest (data not shown), indicating that expected vesicular reuptake was operant and not modified by the intracellular injection of denatured IgG.

Because the reduction of transmitter release can also be produced by modifications of presynaptic Ca^{2+} current (ICa) after the IgG injection, a set of presynaptic voltage-clamp experiments (*n* = 3) was performed to rule out such possibility. Because no reduction or delay in the presynaptic ICa accompanied the reduction in the postsynaptic potential (Fig. 3*A*), we concluded that anti-mSyt I-C2B IgG had no effect on presynaptic ICa.

Spontaneous Transmitter Release. Noise analysis was implemented to further test the hypothesis that the transmitter release reduction observed by presynaptic spike activation and presynaptic voltage-step depolarization was indeed related to decreased transmitter availability. If this finding were to be the case, and spontaneous release is supported by the same pool responsible for the evoked release, spontaneous synaptic noise should
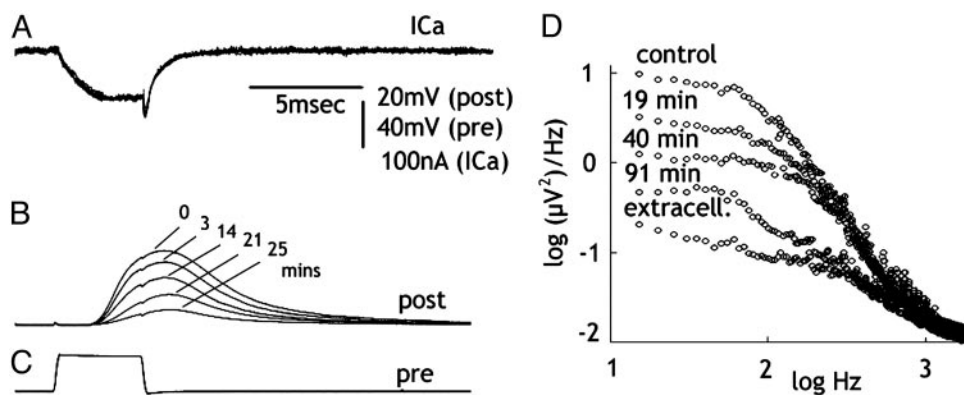
Fig. 3. IgG injection reduces transmitter release and spontaneous synaptic noise without modifying inward Ca^{2+} current. (*A–C*) Reduction of transmitter release (*B*) after a presynaptic voltage-clamp pulse (*C*) at different times after IgG injection. Note the lack of change in ICa (*A*). (*D*) Postsynaptic noise measurements at different times after IgG injection. Control before injection, extracellular noise level with the postsynaptic electrode outside the post axon is shown.

demonstrate similar reduction as the evoked release. Spontaneous release was determined by noise analysis in four synapses (36). In all cases, the reduction of spontaneous synaptic noise correlated well with the reduction in evoked transmitter release. An example of noise reduction is illustrated in Fig. 3*D*. These findings demonstrate a reduction in spontaneous transmitter release that parallel the reduction simultaneously observed in the evoked-release experiments, corroborating the conclusion that anti-mSyt I-C2B IgG reduction is correlated with a decreased transmitter availability.

Two-Photon Confocal Imaging. A two-photon laser-scanning morphological analysis of the giant synapse was performed after presynaptic injection with the fluorescence tagged anti-mSyt I-C2B IgG. During the electrophysiological experiments, the diffusion of the tagged anti-mSyt I-C2B IgG along the preterminal fiber was continuously monitored by using regular fluorescence microscopy, to correlate its progress with possible changes in synaptic release properties. Once the preterminal was totally filled, the electrophysiological protocols described above were implemented. At the end of the electrophysiological experiments, the light-microscopic characteristics of IgG distribution over the presynaptic plasmmalema were determined in 10 synapses.

Two-photon imaging of the injected anti-mSyt I-C2B IgG resulted in well defined clusters of fluorescence that distributed immediately in front of the active-zone site at the inner surface of the plasmalemma (Fig. 4). Their distribution is consistent with the morphological organization of the synaptic vesicle agglomerates at the active zone, where the vesicular-bound Syt is known to be present at high density (7). Whereas a certain amount background fluorescence was always present, given the fact that not all of the IgG becomes bound, the very large difference between background and the signal levels at the synaptic contact and the rather well defined size of the punctate fluorescence imaging agrees with the distribution of Syt I C2B-binding sites at the preterminal synaptic vesicular level. Such arrangement was photographed and is illustrated in Fig. 4 as a montage at low and high magnification.

Morphometry. Quantitative analysis of vesicle counts was determined for three conditions: unstimulated and stimulated at 200 Hz for up to 130 times until all spikes in the stimulus train failed. Both controls and stimulated anti-mSyt I-C2B-injected synapses were treated with the same paradigm. The number of vesicles per active zone in stimulated synapses was approximately half as small as in the unstimulated synapse, 70.93 ± 5.45 ($n = 45$ active

zones). This result is closely comparable with the results from previous work in this preparation with a similar stimulus paradigm (9). Noteworthy differences between unstimulated and stimulated controls were identified in the number of clathrin-coated vesicles (CCVs). Under these two conditions, the number of such CCV profiles was 1.31 ± 0.16 for the unstimulated control condition (Fig. 5*B*) and 3.61 ± 0.33 after high-frequency stimulation ($P < 0.001$) (Fig. 5*D*). After IgG injection, a reduction of vesicular density at the active zone that is further reduced from that observed after repetitive stimulation of noninjected synapses from 41.28 ± 2.73 ($n = 78$) to 27.42 ± 2.33 ($n = 70$ active zones) ($P < 0.01$) occurs. The most distinct and significant finding, however, was the reduction in the number of CCVs within the case of injected terminals (0.82 ± 0.14), which is >4.5 times smaller than that found in noninjected terminals (3.61 ± 0.33; $P < 0.001$) (Fig. 5*F*).

Discussion

The results of this study of the functional role of the C2B domain of Syt I fully support our previous findings (9) by using a different
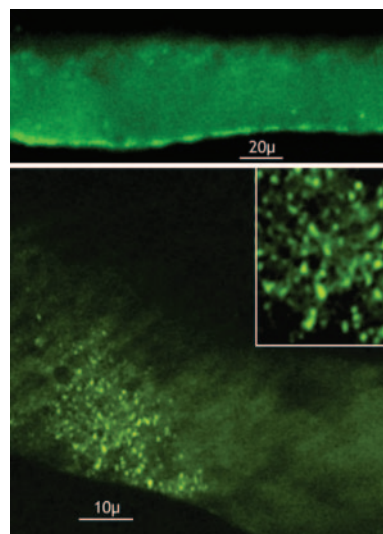

Fig. 4. Presynaptic localization of fluorescent labeled anti-mSyt I-C2B IgG by using two-photon laser-scanning microscopy. (*Upper*) Low-magnification image showing membrane distribution of the fluorescent label. (*Lower* and *Inset*) En phase imaging of the presynaptic membrane, demonstrating the membrane bound distribution of label. Note the distribution corresponds to the size and geometrical distribution of the synaptic active zones in the terminal.
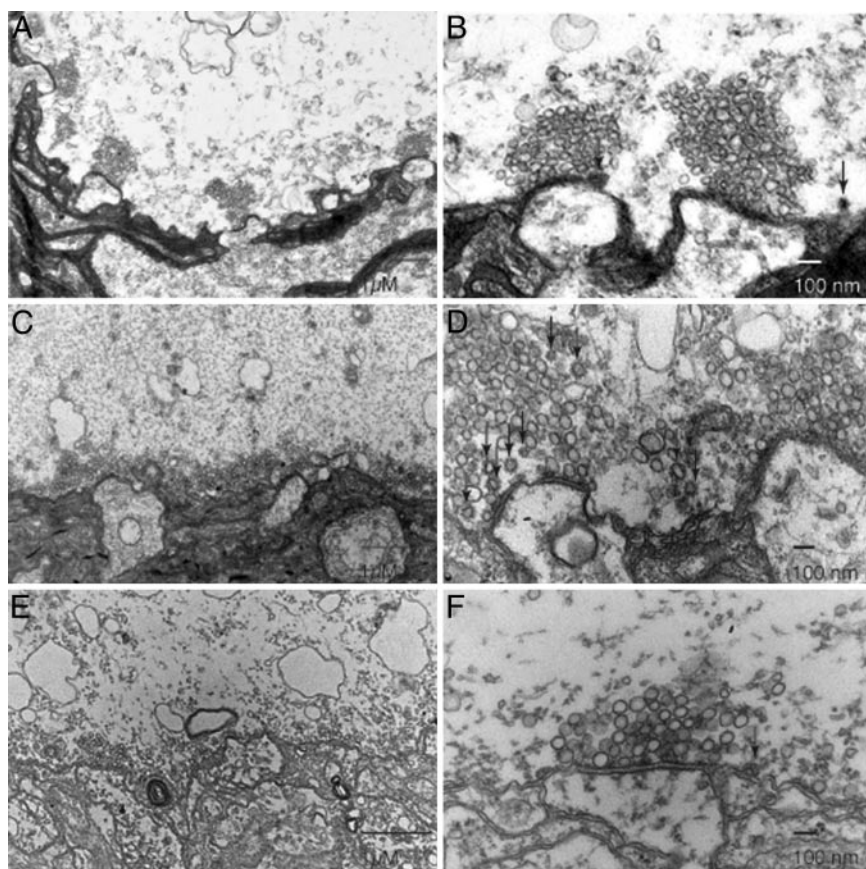
Fig. 5. Presynaptic injection of anti-mSyt I-C2B results in decreased number of CCVs. Ultrastructure of the giant squid synapse identifying the pre- and postsynaptic structures. (*A* and *B*) Electron micrographs from cross sections of nonstimulated, noninjected control synapse. (*A*) A low-magnification image displaying several active zones with large clusters. (*B*) Higher-magnification image illustrating the large number of vesicles and number of CCVs (arrows). (*C* and *D*) Electron micrographs from cross sections of stimulated, noninjected control synapse to illustrate the effect of stimulation on vesicular number and morphological properties. (*C*) Low-magnification image showing a decreased number of vesicles during stimulation. (*D*) An increase in CCVs displayed in higher magnification (arrows). (*E* and *F*) Electron micrographs from cross sections of stimulated, anti-mSyt I-C2B-injected synapse. (*E*) Low-magnification images, demonstrating the significant decreases in vesicle number. (*F*) Display of low number of CCVs in anti-mSyt I-C2B-injected terminals. Arrows identify clathrin-coated vesicles in *B*, *D*, and *F*.

anti-Syt I-C2B IgG. In agreement with our previous results, intraterminal injection blocked vesicular uptake and decreased synaptic transmission due to reduction of vesicular availability at the active zone (Figs. 2 and 5). No interference with the release process was detectable. Furthemore, the two-photon scanning microscopy results demonstrate that the IgG is grouped on the inner surface of plasmalemma in well defined patches that correlated in size and distribution with the synaptic active zone areas (Fig. 4).

Concerning the functional significance of the C2B domain in synaptic transmission; whereas the Ca^{2+}-binding site of the C2B domain of Syt I has recently been shown to be crucial for Ca^{2+}-evoked neurotransmitter release (21, 23), our anti-mSyt I-C2B antibody was neutral for synaptic vesicle exocytosis. The most parsimonious explanation for this discrepancy relates to the fact that the C2B domain exhibits several binding sites, and given that conclusion, anti-Syt I-C2B antibodies may selectively disrupts only given sites. Actually, three distinct ligand-binding sites, with distinct functional roles in synaptic vesicle trafficking, are known to be present in the C2B domain. This domain is composed of an eight-stranded β-sandwich structure (24, 25) (see schematic diagram of Fig. 1*C*). One of the sites consists of two top loops binding one Ca^{2+} ion each, at the C2 sandwich structure (25). A second site consists of a polybasic sequence in the β4 strand (named the C2B effector site) and binds to a

variety of molecules in a Ca^{2+}-independent manner (5). These sites include the clathrin adaptor complex AP-2 (38, 39) and inositol polyphosphates (40). The second C2B effector site is also involved in the Ca^{2+}-dependent self-oligomerization of the C2B domain (17, 39). These two ligand-binding sites are not totally independent, however, because inositol 1,3,4,5-tetrakisphosphate binding to the C2B effector site strongly inhibited Ca^{2+}-dependent self-oligomerization of the C2B domain *in vitro* (17) and Ca^{2+}-binding mutations alter self-oligomerization activity (41). A third site, the conserved WHXL motif in the β8 strand, required for neurexin binding *in vitro* (10, 42), is involved in the attachment of the Syt cytoplasmic domain with plasma membrane in PC12 cells (10, 34), and is involved in synaptic vesicle docking to the active zones in the squid giant synapse (10). During the course of the affinity-purification of the present antibody, the β8 strand antibody was removed by passing through the column coupled with the C terminus of the C2B domain (see *Materials and Methods* for details). Thus, the anti-mSyt I-C2B antibody used in this study is unlikely to inhibit the function of the WHXL motif. Consistent with this hypothesis, we did not observe any defects in the synaptic vesicle docking by the present anti-mSyt I-C2B antibody.

The question remains as to which, if any, binding sites (Ca^{2+}-binding loops or β4 strand) may be masked by our anti-mSyt I-C2B antibody. Because we have previously shown that the

antibody inhibited inositol 1,3,4,5-tetrakisphosphate binding to the C2B domain (9), our anti-mSyt I-C2B antibody should inhibit certain functions of the C2B effector domain; presumably, the interaction of the C2B domain with AP-2 (43) or stonin 2 (44, 45), both of which are involved in clathrin-mediated vesicle endocytosis. Although the polybasic sequence in the C2B effector domain is also required for Ca^{2+}-dependent self-oligomerization (17, 39) and efficient evoked neurotransmitter release (20, 46, 47), our anti-mSyt I-C2B antibody did not inhibit synaptic vesicle exocytosis. The lack of effect of the antibody on synaptic vesicle exocytosis may be attributable to the divalent nature of the whole antibody: the anti-mSyt I-C2B antibody itself oligomerizes the C2B domain, which will promote synaptic vesicle exocytosis (Fig. 1B). By contrast, inositol 1,3,4,5-tetrakisphosphate binding to the C2B domain inhibits Ca^{2+}-dependent self-oligomerization of the C2B domain, which is known to block synaptic vesicle exocytosis (6, 9, 19).

Because the anti-mSyt I-C2B antibody used in this study did not affect synaptic vesicle exocytosis, this polyclonal antibody is unlikely to contain functionally blocking antibody against the Ca^{2+}-binding loops of the C2B domain. If so, why do the Ca^{2+}-binding loops of the C2B domain not act as a good epitope? We propose that Ca^{2+}-binding loops, or their surrounding sequences, are not correctly folded in the "isolated C2B" domain. This finding is the case because the Ca^{2+}-dependent phospholipid-binding activity of the C2B domain requires the adjacent C2A domain (i.e., "tandem C2 domain") (47) and so the Ca^{2+}-binding regions of two C2 domains of Syt III are actually facing each other (24). This fact makes it very difficult to obtain an effective antibody against the Ca^{2+}-binding sites of the C2B domain, which would block synaptic vesicle exocytosis. Production of monoclonal antibody, by using tandem C2 domains as an antigen, is necessary to obtain functionally blocking antibody against the Ca^{2+}-binding sites of the C2B domain. Such a monoclonal antibody may be a useful tool to test the physiological significance of the Ca^{2+}-dependent interaction between the C2B domain and phosphatidylinositol 4,5-bisphosphate, which has recently been proposed to be a crucial process for synaptic vesicle exocytosis (22).

In summary, we have investigated the effect of the anti-mSyt I-C2B antibody on synaptic vesicle trafficking, and found that the antibody selectively blocks synaptic vesicle recycling step rather than synaptic vesicle exocytosis. Our results, together with the previous *in vitro* binding experiments (9, 10, 27, 28), indicate that distinct effector sites in the C2B domain are required for both synaptic vesicle exocytosis and endocytosis.

Note. While this manuscript was being prepared, Grass *et al.* (48) reported that the C2B-AP-2 interaction is mediated by the basic motif in the C2B domain (i.e., C2B effector domain) and depends on the oligomerization of the AP-2 binding site. Therefore, we propose that our anti-mSyt I-C2B antibody restricts AP-2 binding to the oligomerized C2B domain by masking the C2B effector domain, rather than by inhibiting the C2B oligomerization itself.

1. Schiavo, G., Osborne, S. L. & Sgouros, J. G. (1998) *Biochem. Biophys. Res. Commun.* **248,** 1–8.
2. Marquèze, B., Berton, F. & Seagar, M. (2000) *Biochimie* **82,** 409–420.
3. Südhof, T. C. (2002) *J. Biol. Chem.* **277,** 7629–7632.
4. Chapman, E. R. (2002) *Nat. Rev. Mol. Cell Biol.* **3,** 498–508.
5. Fukuda, M. (2003) *Recent Res. Dev. Chem. Phys. Lipids* **1,** 15–51.
6. Llinás, R., Sugimori, M., Lang, E. J., Morita, M., Fukuda, M., Niinobe, M. & Mikoshiba, K. (1994) *Proc. Natl. Acad. Sci. USA* **91,** 12990–12993.
7. Mikoshiba, K., Fukuda, M., Moreira, J. E., Lewis, F. M., Sugimori, M., Niinobe, M. & Llinás, R. (1995) *Proc. Natl. Acad. Sci. USA* **92,** 10703–10707.
8. Mochida, S., Fukuda, M., Niinobe, M., Kobayashi, H. & Mikoshiba, K. (1997) *Neuroscience* **77,** 937–943.
9. Fukuda, M., Moreira, J. E., Lewis, F. M., Sugimori, M., Niinobe, M., Mikoshiba, K. & Llinás, R. (1995) *Proc. Natl. Acad. Sci. USA* **92,** 10708–10712.
10. Fukuda, M., Moreira, J. E., Liu, V., Sugimori, M., Mikoshiba, K. & Llinás, R. R. (2000) *Proc. Natl. Acad. Sci. USA* **97,** 14715–14719.
11. Geppert, M., Goda, Y., Hammer, R. E., Li, C., Rosahl, T. W., Stevens, C. F. & Südhof, T. C. (1994) *Cell* **79,** 717–727.
12. Jorgensen, E. M., Hartwieg, E., Schuske, K., Nonet, M. L., Jin, Y. & Horvitz, H. R. (1995) *Nature* **378,** 196–199.
13. Reist, N. E., Buchanan, J., Li, J., DiAntonio, A., Buxton, E. M. & Schwarz, T. L. (1998) *J. Neurosci.* **18,** 7662–7673.
14. Poskanzer, K. E., Marek, K. W., Sweeney, S. T. & Davis, G. W. (2003) *Nature* **426,** 559–563.
15. Schiavo, G., Stenbeck, G., Rothman, J. E. & Söllner, T. H. (1997) *Proc. Natl. Acad. Sci. USA* **94,** 997–1001.
16. Earles, C. A., Bai, J., Wang, P. & Chapman, E. R. (2001) *J. Cell Biol.* **154,** 1117–1123.
17. Fukuda, M., Kabayama, H. & Mikoshiba, K. (2000) *FEBS Lett.* **482,** 269–272.
18. Littleton, J. T., Bai, J., Vyas, B., Desai, R., Baltus, A. E., Garment, M. B., Carlson, S. D., Ganetzky, B. & Chapman, E. R. (2001) *J. Neurosci.* **21,** 1421–1433.
19. Fukuda, M., Katayama, E. & Mikoshiba, K. (2002) *J. Biol. Chem.* **277,** 29315–29320.
20. Zhang, X., Kim-Miller, M. J., Fukuda, M., Kowalchyk, J. A. & Martin, T. F. J. (2002) *Neuron* **34,** 599–611.
21. Mackler, J. M., Drummond, J. A., Loewen, C. A., Robinson, I. M. & Reist, N. E. (2002) *Nature* **418,** 340–344.
22. Bai, J., Tucker, W. C. & Chapman, E. R. (2004) *Nat. Struct. Mol. Biol.* **11,** 36–44.
23. Nishiki, T. & Augustine, G. J. (2004) *J. Neurosci.* **24,** 8542–8550.
24. Sutton, R. B., Ernst, J. A. & Brunger, A. T. (1999) *J. Cell Biol.* **147,** 589–598.
25. Fernandez, I., Arac, D., Ubach, J., Gerber, S. H., Shin, O., Gao, Y., Anderson, R. G. W., Südhof, T. C. & Rizo, J. (2001) *Neuron* **32,** 1057–1069.
26. Sutton, R. B., Davletov, B. A., Berghuis, A. M., Südhof, T. C. & Sprang, S. R. (1995) *Cell* **80,** 929–938.
27. Fukuda, M., Kojima, T., Aruga, J., Niinobe, M. & Mikoshiba, K. (1995) *J. Biol. Chem.* **270,** 26523–26527.
28. Fukuda, M., Yamamoto, A. & Mikoshiba, K. (2001) *J. Biol. Chem.* **276,** 41112–41119.
29. Ubach, J., Lao, Y., Fernandez, I., Arac, D., Südhof, T. C. & Rizo, J. (2001) *Biochemistry* **40,** 5854–5860.
30. Fukuda, M., Kanno, E. & Mikoshiba, K. (1999) *J. Biol. Chem.* **274,** 31421–31427.
31. Fukuda, M. & Mikoshiba, K. (2000) *J. Biol. Chem.* **275,** 28180–28185.
32. Fukuda, M., Kanno, E., Ogata, Y. & Mikoshiba, K. (2001) *J. Biol. Chem.* **276,** 40319–40325.
33. Fukuda, M. & Mikoshiba, K. (2001) *J. Biol. Chem.* **276,** 27670–27676.
34. Fukuda, M. & Mikoshiba, K. (1999) *J. Biol. Chem.* **274,** 31428–31434.
35. Sugimori, M., Tong, C.-K., Fukuda, M., Moreira, J. E., Kojima, T., Mikoshiba, K. & Llinás, R. (1998) *Neuroscience* **86,** 39–51.
36. Lin, J. W., Sugimori, M., Llinás, R. R., McGuinness, T. L. & Greengard, P. (1990) *Proc. Natl. Acad. Sci. USA* **87,** 8257–8261.
37. Llinás, R., Steinberg, I. Z. & Walton, K. (1981) *Biophys. J.* **33,** 289–321.
38. Mizutani, A., Fukuda, M., Niinobe, M. & Mikoshiba, K. (1997) *Biochem. Biophys. Res. Commun.* **240,** 128–131.
39. Chapman, E. R., Desai, R. C., Davis, A. F. & Tornehl, C. K. (1998) *J. Biol. Chem.* **273,** 32966–32972.
40. Fukuda, M., Aruga, J., Niinobe, M., Aimoto, S. & Mikoshiba, K. (1994) *J. Biol. Chem.* **269,** 29206–29211.
41. Desai, R. C., Vyas, B., Earles, C. A., Littleton, J. T., Kowalchyck, J. A., Martin, T. F. J. & Chapman, E. R. (2000) *J. Cell Biol.* **150,** 1125–1136.
42. Perin, M. S. (1994) *J. Biol. Chem.* **269,** 8576–8581.
43. Zhang, J. Z., Davletov, B. A., Südhof, T. C. & Anderson, R. G. W. (1994) *Cell* **78,** 751–760.
44. Martina, J. A., Bonangelino, C. J., Aguilar, R. C. & Bonifacino, J. S. (2001) *J. Cell Biol.* **153,** 1111–1120.
45. Walther, K., Diril, M. K., Jung, N. & Haucke, V. (2004) *Proc. Natl. Acad. Sci. USA* **101,** 964–969.
46. Mackler, J. M. & Reist, N. E. (2001) *J. Comp. Neurol.* **436,** 4–16.
47. Bai, J., Wang, P. & Chapman, E. R. (2002) *Proc. Natl. Acad. Sci. USA* **99,** 1665–1670.
48. Grass, I., Thiel, S., Honing, S. & Haucke, V. (October 18, 2004) *J. Biol. Chem.*, 10.1074/jbc.M409995200.